4

Nanomagnetic materials and devices

4.1 MAGNETISM

Nanotechnology as a term applied in the field of magnetism may be regarded as either relatively mature, or as a subject at a nascent stage in its development. Many of the permanent magnets in common use today, in devices ranging from high-efficiency motors to fridge magnets, have properties dictated by the physical nanostructure of the material, and the subtle and complex magnetic interactions that this produces. The use of nanostructured magnets has already enabled very significant savings in energy consumption and weight for motors, which contributes strongly to the green economy. Data storage density has increased with a compound growth rate of 60%, giving (in 2004) disk drives for the mass PC market in excess of 400 Gbyte. The internet, image handling in cameras and data storage drive the demand for increases in data storage capacity. Fujitsu recently demonstrated (spring 2002) 100 Gbit/in^2 data storage capacity in a form of conventional longitudinal recording media. This requires an effective 'bit size' of 80 nm square. Figure 4.1 is a reproduction of an IBM road map (dated 2000) for the projected development of storage capacity. There are fundamental physical barriers to be overcome (see the superparamagnetic limit discussed in Section 4.1.4) in order to keep to this road map for increasing capacity with current technologies, and a paradigm shift will be needed which will be nanotechnology led.

We begin this chapter with a brief introduction to the *language* and *technical terms* involved in the study of nanomagnetism. There are many suitable texts which may be consulted to provide a more extensive coverage of the background. These are listed in the bibliography at the end of the chapter.

4.1.1 Magnetostatics

In common usage, magnetic materials are those that exist in a state of permanent magnetization without the need to apply a field. For all permanent magnets there is a

Nanoscale Science and Technology Edited by R. W. Kelsall, I. W. Hamley and M. Geoghegan

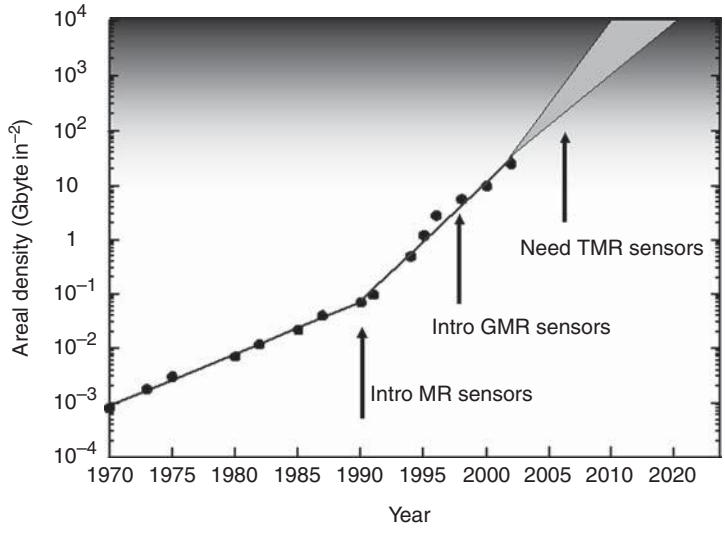

Figure 4.1 Schematic data storage road map drawn up from various internet sources. The introduction of new recording head technologies (magnetoresistance plus giant and tunnelling magnetoresistance) is marked by the arrows

north pole (N) and a south pole (S), and lines of magnetic field pass from N to S. If we begin with the simple premise that the net properties of a magnet are some form of sum over a large number of atomic or electronic magnets (referred to as magnetic dipole moments), we can separate magnetic materials into three categories.

4.1.2 Diamagnetism, paramagnetism and ferromagnetism

There are three categories of magnetism that we need to consider: diamagnetism, paramagnetism and ferromagnetism. Diamagnetism is a fundamental property of all atoms (molecules), and the magnetization is very small and opposed to the applied magnetic field direction. Many materials exhibit paramagnetism, where a magnetization develops parallel to the applied magnetic field as the field is increased from zero, but again the strength of the magnetization is small. In the language of the physicist, ferromagnetism is the property of those materials which are intrinsically magnetically ordered and which develop spontaneous magnetization without the need to apply a field. The ordering mechanism is the quantum mechanical exchange interaction. It is this final category of magnetic material that will concern us in this chapter. A variation on ferromagnetism is ferrimagnetism, where different atoms possess different moment strengths but there is still an ordered state below a certain critical temperature.

We will now define some key terms. The magnetic induction **B** has the units of tesla (T). To give a scale, the horizontal component of the earth's magnetic flux density is approximately $20\,\mu$T in London; stray fields from the cerebral cortex, are about 10 fT. The magnetic field strength **H** can be defined by

$$\mathbf{B} = \mu_0 \mathbf{H}, \tag{4.1}$$

where $\mu_0 = 4\pi \times 10^{-7}\mathrm{H\,m^{-1}}$ is the permeability of free space. This gives the horizontal component of the earth's magnetic field strength as approximately $16\,\mathrm{A\,m^{-1}}$ in London. The flux $\Phi = BA$ can be defined, where A is a cross-sectional area. Flux has the units of weber (W).

If a ferromagnetic material is now placed in a field **H**, Equation (4.1) becomes

$$\mathbf{B} = \mu_0(\mathbf{H} + \mathbf{M}) = \mu_0(\mathbf{H} + \chi\mathbf{H}) = \mu_r\mu_0\mathbf{H}, \tag{4.2}$$

where **M** is the magnetization of the sample (the magnetic dipole moment per unit volume). We define χ as the susceptibility of the magnetic material, and $\mu_r = 1 + \chi$ as the relative permeability of the material (both χ and μ are dimensionless). Table 4.1 summarizes this classification scheme, and gives values for typical susceptibilities in each category.

If we take *any* ferromagnet and increase the field from zero to some peak value, decrease the field back through zero to an equal and opposite value and then return again to the original peak value, we trace out the hysteresis loop (Figure 4.2). The name 'hysteresis' comes from the Greek for loss. Energy is dissipated in traversing the loop. This energy loss is primarily manifested as heat. There are several key points on the loop. The saturation magnetization $\mathbf{M}_s$ is the maximum value that the magnetic dipole moment per unit volume can take in the direction of an applied magnetic field. In this state all the contributing atomic (electronic) moments are aligned in the field direction.

Table 4.1 Classification of magnetic materials by susceptibility

Diamagnet ($\chi < 0$)	**Paramagnet ($\chi > 0$)**	**Ferromagnet ($\chi \gg 0$)**
Cu: -0.11×10^{-5}	Al: 0.82×10^{-5}	Fe: $>10^2$
Au: -0.19×10^{-5}	Ca: 1.40×10^{-5}	
Pb: -0.18×10^{-5}	Ta: 1.10×10^{-5}	

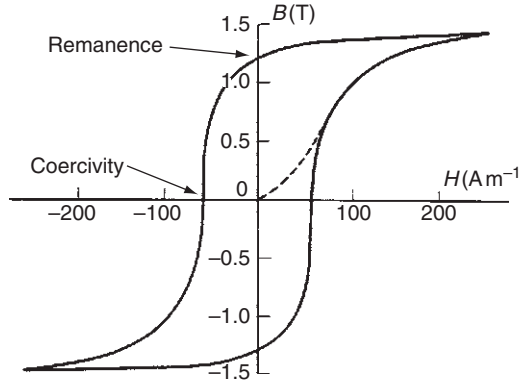

Figure 4.2 A schematic diagram of a magnetization (or hysteresis) loop. Remanence is the magnetization remaining when the field is reduced to zero from that required to saturate the sample. Coercivity is the field required to bring the magnetization to zero from remanence

The remanent magnetization $\mathbf{M}_r$ is the magnetization remaining in the sample when the applied field is reduced to zero from the value which saturated the sample. The coercivity $\mathbf{H}_c$ is the field required to reduce the magnetization to zero from saturation (Figure 4.2), and is applied in the opposite direction to the original saturating field. If the magnetization is reduced to zero from less than its saturating value then $\mathbf{H}_c$ is termed the coercive field (always less than the coercivity). The ratio M_r/M_s and the area enclosed in the loop are important in determining the applicability of a given ferromagnet (Section 4.2).

4.1.3 Magnetic anisotropy

If we take a *single crystal* of a ferromagnet, and apply a magnetic field along different crystallographic directions, the magnetization varies with field depending on the chosen direction for the applied field (Figure 4.3). This phenomenon goes under the generic title of magnetic anisotropy. For Fe, as shown in Figure 4.3, ⟨100⟩ are the easy directions (low field required to saturate), ⟨110⟩ and ⟨111⟩ directions are hard (high field to saturate). This form of anisotropy is termed magnetocrystalline anisotropy and is closely related to the detailed electronic structure of the crystal.

Fe is a body-centred cubic solid; that is, the Fe atoms arrange on the cube corners and at each cube centre in a regular three-dimensional pattern. The ⟨100⟩ directions are along a cube edge, the ⟨110⟩ directions along a face diagonal and the ⟨111⟩ directions along a cube body diagonal.

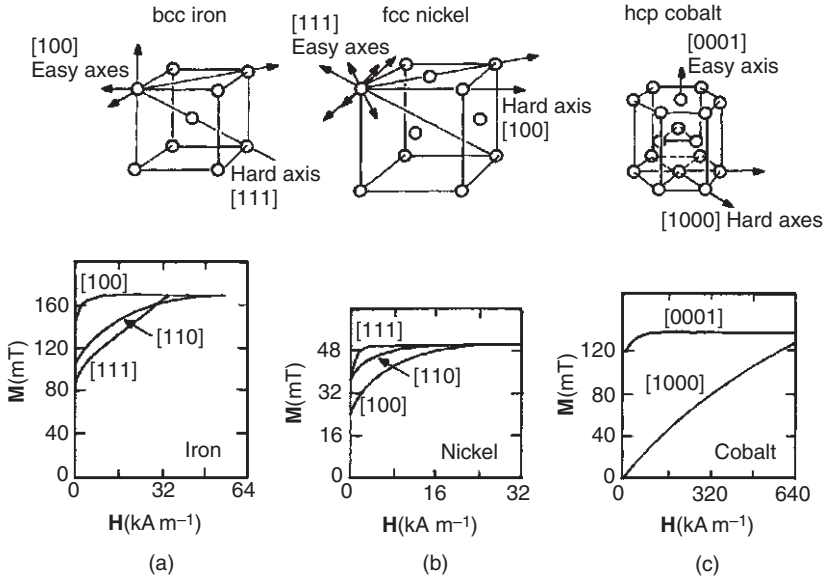

Figure 4.3 The crystal structure and magnetization loops For Fe, Ni and Co, demonstrating the anisotropic nature of the magnetization process. After R. C. O'Handley, *Modern Magnetic Materials: Principles and Applications*, Wiley, New York, 2000, p. 180. Copyright 2000 John Wiley & Sons Inc.

In certain crystals such as cobalt, which has a hexagonal closed-packed (hcp) crystal structure, there is only one easy axis (in this case perpendicular to the close-packed plane; see Figure 4.10 for another example), leading to uniaxial anisotropy. The magnetocrystalline anisotropy energy is a minimum when the magnetization lies along this easy axis. The magnetocrystalline anisotropy energy is a maximum when the magnetization is at 90° to the easy axis. We can express this anisotropy energy E_a by expanding in terms of material-dependent anisotropy constants K_i using a series of powers of $\sin^2\theta$ (to reflect the symmetry), where θ is the angle between the easy axis and the magnetization:

$$E_a = K_0 + K_1 \sin^2\theta + K_2 \sin^4\theta + \ldots \tag{4.3}$$

In all expressions for anisotropy energy there is a constant term K_0. This term is ignored, as in practice it is changes in energy due to moment rotations that are of interest. For a given crystal class (e.g., cubic) direction cosines (α_i) related to the cube edges are used to define the direction of magnetization. The anisotropy energy is then expanded in a polynomial series involving the α_i. By symmetry arguments (for details see books listed in the bibliography)

$$E_a = K_1\left(\alpha_1^2\alpha_2^2 + \alpha_2^2\alpha_3^2 + \alpha_1^2\alpha_3^2\right) + K_2\left(\alpha_1^2\alpha_2^2\alpha_3^2\right) + \ldots \tag{4.4}$$

There can also be a magnetic anisotropy associated with the shape of a magnetic material; it has its origins in the demagnetizing field H_d within the material. Magnetic field lines always run from north poles to south poles, and so *inside* a magnet there is a field in the opposite direction to the magnetization induced by an external field. This reduces the net field experienced by the magnet.

We now rewrite Equation (4.2) to take account of this field internal to the magnet and opposite in direction to the magnetization

$$\mathbf{B} = \mu_0\mathbf{H}_a + \mu_0\mathbf{M} - \mu_0\mathbf{H}_d. \tag{4.5}$$

In the absence of an applied field, $\mathbf{H}_a = \mathbf{0}$, the magnetostatic energy per unit volume, E_s, is given by

$$E_s = \frac{1}{2}\mathbf{B}\cdot\mathbf{M}, \qquad \mathbf{B}_i = \mu_0\mathbf{H}_d = \mu_0 N_d\mathbf{M}, \tag{4.6}$$

where $0 \le N_d \le 1$ is the geometrically defined demagnetizing factor. The factor 1/2 is to ensure that each dipole interaction with the field is counted only once. For a prolate spheroid, taking the major axis (c) as the easy axis, we have

$$E_s = \frac{1}{2}\left((M\cos\theta)^2 N_c + (M\sin\theta)^2 N_a\right)\mu_0 = \frac{1}{2}\mu_0 N_c M^2 + \frac{1}{2}\mu_0(N_a - N_c)M^2\sin^2\theta. \tag{4.7}$$

This should be compared with Equation (4.3), and allows us to define K_s as the shape anisotropy constant. In this case:

$$K_s = \frac{1}{2}\mu_0(N_a - N_c)M^2. \tag{4.8}$$

For a sphere $N_a = N_c$ and $K_s = 0$ and there are no easy directions due to shape anisotropy.

It is now obvious that as physical dimensions are decreased, and we start to produce magnetic materials with one or more dimensions on the nanometre scale, the possibility of significant anisotropy due to shape increases. It is very important to remember that when more than one type of anisotropy is present they do not add vectorially, rather one type of anisotropy will be dominant, determining the local direction of magnetization in the absence of a magnetic field.

When a ferromagnet undergoes a change in the state of magnetization there may be an accompanying change in physical dimensions (the Joule effect). A fundamental material constant can be defined, the saturation magnetostriction constant λ_s, which decreases with temperature, approaching zero at $T = T_c$. T_c is the Curie temperature, and is the temperature above which thermal energy is sufficient to overcome the moment alignment produced by the exchange interaction. The measured strain depends on the crystallographic direction for the measurement. When the distance, r, between two atomic magnetic moments can vary, the interaction energy must in general be a function of r and ϕ, where ϕ is the angle between the magnetic moments (assumed parallel due to exchange) and the bond axis. The crystal lattice will therefore be deformed when ferromagnetism is established ($T < T_c$); this is the spontaneous magnetostriction. As the angle ϕ is varied (say by applying a field at an angle to an easy direction) the interaction energy may also change (this is magnetic anisotropy) and there may be an accompanying change in r to keep the total energy a minimum. This is termed field-induced magnetostriction. There is a fundamental link between anisotropy and magnetostriction; magnetostriction is related to the strain derivative of the anisotropy energy.

A phenomenological model can be produced which relates the field-induced strain to fundamental magnetostriction constants and angles in a crystal. It can be shown (see bibliography) that for a cubic crystal:

$$\lambda_{si} = \frac{3}{2}\lambda_{100}\left(\alpha_1^2\beta_1^2 + \alpha_2^2\beta_2^2 + \alpha_3^2\beta_3^2 - \frac{1}{3}\right) + 3\lambda_{111}(\alpha_1\alpha_2\beta_1\beta_2 + \alpha_2\alpha_3\beta_2\beta_3 + \alpha_3\alpha_1\beta_3\beta_1). \tag{4.9}$$

λ_{si} is the strain from the ideal demagnetized state to saturation, α_i are the direction cosines defining the applied field direction, and β_i are the direction cosines defining the strain direction. To determine the strain in the same direction as the magnetization, put $\alpha_1\alpha_2\alpha_3 = \beta_1\beta_2\beta_3$ in Equation (4.9) to give:

$$\lambda_{si} = \lambda_{100} + 3(\lambda_{111} - \lambda_{100})\left(\alpha_1^2\alpha_2^2 + \alpha_2^2\alpha_3^2 + \alpha_3^2\alpha_1^2\right). \tag{4.10}$$

λ_{si} is uniquely defined and is a fundamental property (however the demagnetized state is hard to uniquely define in theory or in practice).

Just as the presence of magnetostriction may cause a dimensional change as the magnetization varies in an applied field, so an applied strain may cause a change in magnetization (inverse Joule or Villari effect). An easy direction may be defined associated with the applied strain (or stress).

When one or more dimensions of a magnetic material is on the nanometre scale, the surface area to volume ratio must increase. The atomic relaxations at free surfaces and the lattice strains at interfaces may thus have a profound effect on anisotropy and magnetostriction in nanoscale magnetic materials. More will be said about this later.

4.1.4 Domains and domain walls

If elements such as iron(Fe) are ferromagnetic, that is all the moments are aligned as a result of the exchange force, why is it that not all pieces of iron behave like permanent magnets? Consider a block of ferromagnet magnetized to saturation; from earlier we have that the magnetostatic energy E_s for a sample volume V is

$$E_s = \frac{1}{2}\mu_0 N_d M_s^2 V. \tag{4.11}$$

For Fe, $M_s = 1.73 \times 10^6\,\mathrm{A\,m^{-1}}$; taking $N_d = 1/3$ and $V = 10^{-6}\,\mathrm{m^3}$, $E_s = 0.627\,\mathrm{J}$ in this saturated state. If the sample is allowed to divide into two regions (domains) of equal volume but opposite directions of magnetization, then

$$E \approx \frac{1}{2}E_s + \gamma_w A_w, \tag{4.12}$$

where γ_w is the energy per unit area of the 'wall' separating the domains and A_w is the wall area. The factor 1/2 comes in as before, to avoid counting interactions twice. For Fe: $\gamma_w = 1.24 \times 10^{-3}\,\mathrm{J\,m^{-2}}$, and $E = 0.314\,\mathrm{J}$. Division into further domains to reduce E will continue until it costs more energy to create another wall than is gained by division:

$$E \approx \frac{1}{n}E_s + (n-1)\gamma_w A_w, \tag{4.13}$$

where n is the number of domains in the sample. Figure 4.4 is a schematic diagram of what is happening. E can be reduced further by the formation of closure domains,

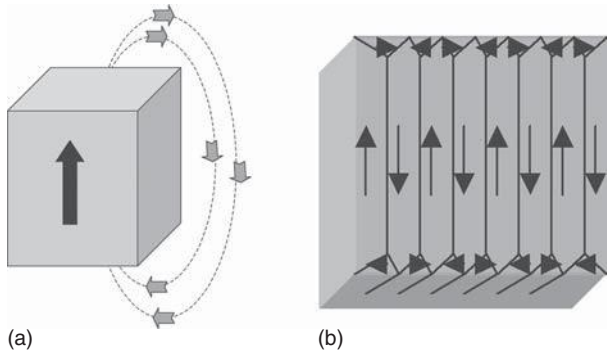

Figure 4.4 (a) A single-domain ferromagnetic particle, (b) a multidomain ferromagnetic particle with closure domains on the top and bottom surfaces

which remove the presence of free poles from the sample surface. In a domain, all the moments are aligned (i.e., locally the sample is magnetized to saturation by the exchange interaction). A neighbouring domain may be magnetized in a different direction (but still locally to saturation, and usually with the moments in an easy direction).

We need to consider how the direction of magnetization varies across the boundary between two domains. This reduces the question to how local anisotropies and exchange interactions compete to determine the direction of the local magnetic moment. We obtain a basic picture from energy considerations. If two neighbouring magnetic moments are not aligned with each other, some exchange energy is stored:

$$E_{\text{ex}} = -2JS^2 \cos\phi, \tag{4.14}$$

where J is the exchange integral and S is the spin quantum number. If ϕ is small (justified later) then:

$$\cos\phi = 1 - \frac{\phi^2}{2} + \frac{\phi^4}{24} - \cdots \quad \text{and} \quad E_{\text{ex}} = 2JS^2\frac{\phi^2}{2} - 2JS^2. \tag{4.15}$$

If the domain wall is abrupt (i.e., the moments rotate from one domain direction to another from one lattice site to the next) then a large exchange energy is stored. Exchange energy considerations taken on their own argue in favour of a wide domain wall with the moments rotating slowly from site to site. If the rate of moment rotation across the wall is slow, the *extra* energy stored due to the presence of the domain wall is

$$E_{\text{ex}} = JS^2\phi^2 \text{ per spin pair.} \tag{4.16}$$

It is more useful to know the exchange energy per unit wall area, and to estimate this energy we consider a simple cubic lattice of side a and a plane domain wall parallel to a cube face of thickness N atoms. There are $1/a^2$ rows of N atoms per unit wall area. If γ_{ex} is the energy per unit wall area:

$$\gamma_{\text{ex}} = \frac{JS^2N\phi^2}{a^2} = \frac{JS^2\pi^2}{Na^2} \tag{4.17}$$

for a 180° domain wall (i.e., $\phi_{\text{total}} = \pi$ radians) and equal increments in ϕ from site to site (i.e., $\phi = \pi/N$).

In zero applied field, the moments within a domain usually lie in easy directions. In the domain wall, the moments are usually directed away from easy directions. Hence anisotropy energy is stored in the region of the domain wall. Also, the presence of anisotropy energy favours a narrow domain wall (few moments out of easy directions):

$$E_{\text{an}} = K_1 \times \text{volume of the wall.} \tag{4.18}$$

Let γ_{an} be the anisotropy energy stored per unit wall area:

$$\gamma_{\text{an}} = K_1Na. \tag{4.19}$$

The total wall energy per unit area, γ, can then be written as:

$$\gamma = \gamma_{ex} + \gamma_{an} = \frac{JS^2\pi^2}{Na^2} + K_1 Na. \tag{4.20}$$

The domain wall thickness may be de defined by $\delta = Na$, and then minimization of γ with respect to δ yields

$$\frac{d\gamma}{d\delta} = -\frac{JS^2\pi^2}{\delta^2 a} + K_1 = 0, \quad \text{where} \quad \delta = \left(\frac{JS^2\pi^2}{Ka}\right)^{1/2} = \sqrt{\frac{A}{K_1}} \quad \text{and} \quad \gamma = 2K\delta \propto \sqrt{AK_1}. \tag{4.21}$$

A is called the exchange stiffness; typical values are $\delta = 120$ atoms, $\gamma = 3\,\mathrm{mJ\,m^{-2}}$. The energy balances can change when one or more dimension is reduced in to the nanometre range so that shape anisotropy becomes significant.

The domain wall in Figure 4.5 is approximated by an elliptical cylinder of width W and height D. If $W > D$ the demagnetising energy flips the wall into Néel mode. Here the magnetization is constrained to rotate in the plane of the film. This reduces the magnetostatic contribution to the total energy. A 90° Néel wall has less energy than a 180° Bloch wall. Further energy minimization can be achieved by forming cross-tie walls which further reduce magnetostatic terms in the energy.

By further examining the total energy, it is possible to see that there are cases where it is energetically unfavourable to divide into domains. Take a uniformly magnetized sphere of radius r and divide it into two domains:

$$E_{s-2domains} \approx \frac{1}{2} E_{s-1domain}. \tag{4.22}$$

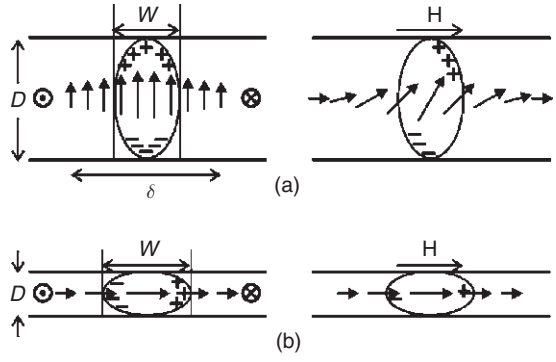

Figure 4.5 Schematic diagrams of Bloch and Néel domain walls represented by regions enclosed by the ellipses. Redrawn after A. Hubert and R. Schäfer, *Magnetic Domains*, Springer, 1998, p. 239 with permission Copyright 1998 Springer-Verlag. (a) In the Bloch wall, the magnetic moments (represented by the arrows) rotate in a plane perpendicular to the sample surface, resulting in N (+) and S (−) poles on the surfaces. (b) In the Néel wall, the moments in the wall rotate in the sample plane, giving rise to no surface poles. The direction of the magnetization in the domains is out of the plane of the paper but in the sample plane, as marked by the circles dots and crosses

To create two domains, the domain wall energy $\pi r^2\gamma$ is added. If

$$E_s \leq \frac{E_s}{2} + \pi r^2\gamma \tag{4.23}$$

there is no division into domains as there is no net energy reduction. For a sphere:

$$\left(\frac{1}{4}\mu_0 N_d M^2\right)\left(\frac{4}{3}\pi r^3\right) \leq \pi r^2\gamma, \quad \text{implying} \quad r \leq \frac{9\gamma}{\mu_0 M^2} \text{ for } N_d = 1/3. \tag{4.24}$$

For Fe_3O_4 the critical radius below which there is only a single domain is $r \leq 6\,\text{nm}$. We can therefore conclude that making nanoscale magnetic materials may result in changes to the bulk domain structure, or even the inability to create domain walls at all.

In the regime of single-domain physics, as the particle size reduces further, the total free energy contribution from the magnetization approaches $k_B T$ (0.025 eV at room temperature). In this case the magnetization may change direction under thermal excitation in the absence of a field. This is the so-called superparamagnetic limit. This limit presents a barrier to the continuous decrease in magnetic particle size whilst retaining stability in the magnetization.

4.1.5 The magnetization process

Magnetic materials often experience applied fields that change both magnitude and direction with time. As can be seen from Figure 4.2, the behaviour is very complex; plotting B or M against H yields curves of this generic form for all magnetic materials. Hard magnetic materials require high remanence and coercivity but soft magnetic materials require low coercivity and low anisotropy. At the fundamental level it is the direction and magnitude of anisotropies, and the ease or difficulty of moving domain walls through the sample, that determine whether a particular sample class is magnetically hard or soft. As a rule of thumb, soft magnetic materials have coercivities below $1\,\text{kA m}^{-1}$ and anisotropy energy densities less than $1\,\text{kJ m}^{-3}$. Hard magnetic materials would have coercivities and anisotropy energy densities higher than these values.

Over the past twenty years, the nanostructure of alloys has come under sufficient control by process developments and subtle variations of alloy chemistry, that record hard ($H_c > 2 \times 10^6\,\text{A m}^{-1}$) and soft ($H_c < 1\,\text{A m}^{-1}$) magnetic materials can be produced. We now demonstrate this by considering some specific examples of nanomagnetic materials.

4.2 NANOMAGNETIC MATERIALS

A broad classification of nanomagnetic materials may be made as follows:

- *Particulate nanomagnets*: granular solids where one or more phases are magnetic; nanograined layers grown on columnar films; quasi-granular films made by heat-treating multilayers of immiscible solids.

- *Geometrical nanomagnets*: columnar films or nanowires; needle-shaped particles in a matrix.
- *Layered nanomagnets*: multilayers with metallic and/or other nanometre-thick films on a supporting substrate (Section 4.2.2).

4.2.1 Particulate nanomagnets

Rapid solidification processing can be regarded in essence as an exercise in basic calorimetry. If a hot body (small melt puddle) and a cold body (large chill block) are brought together, the resultant temperature will lie between the two and will tend towards that of the larger thermal mass (chill block). Cooling rates of order $10^6\,\mathrm{K\,s^{-1}}$ are easily achieved in the laboratory.

There are two routes to producing nanophase material in this way: (1) form an amorphous phase then heat-treat to develop the nanostructure; (2) cool more slowly so that the nanostructure is developed without further treatment. The alloy chemistry can be varied to go from the softest (lowest coercivity and anisotropy) to the hardest (highest coercivity and anisotropy) magnetic materials known:

$$\text{soft} = \text{FeCuNbSiB} \Rightarrow \text{NdFeB} = \text{hard}.$$

For soft ferromagnets $Fe_{73.5}B_9Si_{13.5}Nb_3Cu$ is the archetype, going under the trade name FINEMET. The nanostructure comes about as Cu enhances crystal nucleation, producing many centres for crystals to form. The presence of Nb retards crystal growth, stopping the grains growing on the nucleation centres. The result is bcc-Fe_3Si grains of size 10–15 nm in an amorphous ferromagnetic matrix. A more detailed discussion of the nanostructure formation of FINEMET is included in Section 5.3.2.

It is the physical nanostructure and the resultant interplay between exchange and anisotropy energies that is significant here. In very small grains that are magnetically coupled, exchange forces cause the moments in neighbouring grains to lie parallel, overcoming the intrinsic easy-axis properties of the individual grains. The coupling dominates over length scales shorter than the exchange length, L_{ex}, for given exchange stiffness, A. This length is of the order of the domain wall width defined earlier, and is an expression for the length scale over which the direction of magnetization can vary:

$$L_{ex} = \sqrt{\frac{A}{K_1}} = 35\,\text{nm for } Fe_3Si. \tag{4.25}$$

We can make a simple model of this coupling using the *random anisotropy model*. Figure 4.6 is a schematic diagram of square nanograins, showing the magnetization direction wandering from grain to grain. Starting with a grain size D, and each grain having anisotropy constant K_1, it is assumed that the anisotropy directions are random from grain to grain. The effective anisotropy $\langle K \rangle$ results from averaging over $N = (L_{ex}/D)^3$ grains in a volume $V = L_{ex}^3$. For a finite number of grains there will always be some net

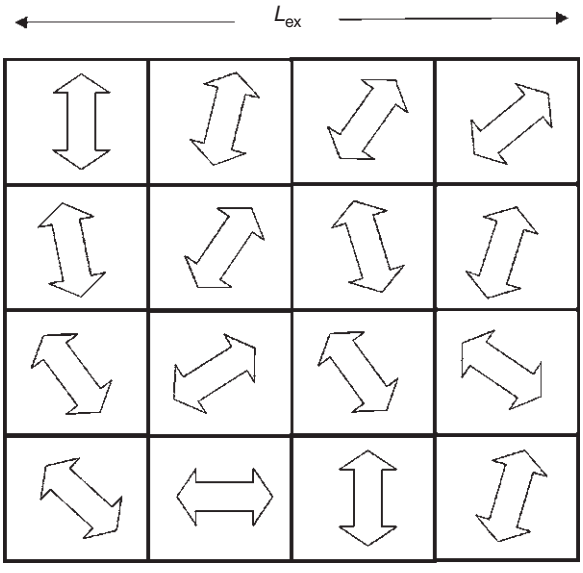

Figure 4.6 A schematic illustration of a nanostructured soft ferromagnet. Each square represents one grain, and the block arrows represent the direction of magnetization within each grain. L_{ex} is the exchange length

easy direction defined by an effective anisotropy constant $\langle K \rangle$. $\langle K \rangle$ is the mean anisotropy fluctuation amplitude of the grains and is given by:

$$\langle K \rangle \approx \frac{K_1}{\sqrt{N}} = K_1 \left(\frac{D}{L_{ex}} \right)^{3/2}. \tag{4.26}$$

From Equation (4.25) with K_1 replaced by $\langle K \rangle$ we have:

$$\langle K \rangle \approx \frac{K_1^4}{A^3} D^6. \tag{4.27}$$

Figure 4.7 is a schematic diagram of how the strength of local anisotropy energy interacts with the exchange energy, demonstrating the extremes of spin alignment for weak and strong local anisotropy energy. If the local anisotropy is strong, the magnetization is well aligned whereas for weak local anisotropy, the magnetization changes direction gradually, effectively overcoming the direction of the local anisotropy. The weak anisotropy limit is relevant for soft nanophase magnets. Figure 4.8 shows the variation of coercivity with grain size, the coercivity being directly proportional to $\langle K \rangle$. The D^6 law (4.27) is clearly obeyed over a range of nanometric grain sizes. Figure 4.9 illustrates how the annealing temperature must be carefully chosen to ensure that the correct microstructure (that required for low coercivity) is produced. The optimum conditions produce iron–silicon grains a few tens of nanometres in diameter surrounded by a magnetically soft amorphous matrix. This produces the behaviour seen in the lower part of Figure 4.7.

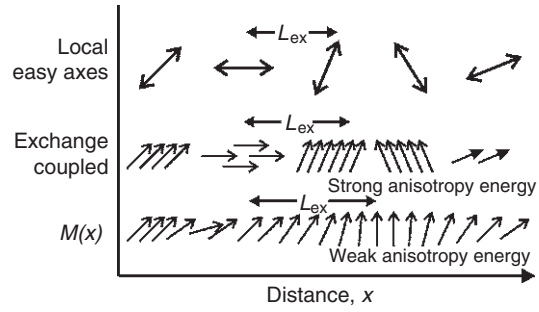

Figure 4.7 A schematic diagram of how the exchange and anisotropy strengths interplay to determine the net exchange length in a nanomagnet. Redrawn after R. C. O'Handley, *Modern Magnetic Materials: Principles and Applications*, Wiley, New York, 2000, p. 337. Copyright 2000, with permission of John Wiley & Sons Inc.

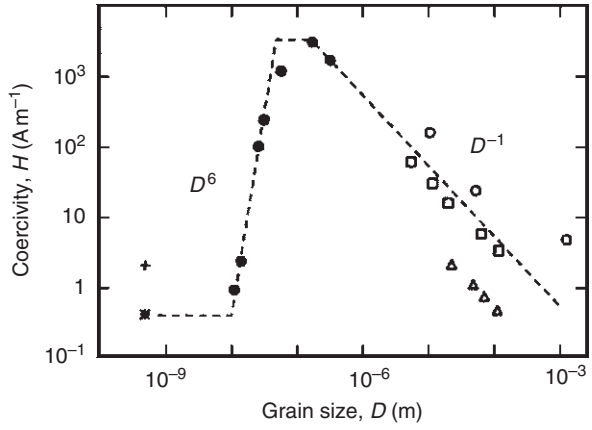

Figure 4.8 The variation of coercivity with grain size in five soft magnetic alloys. Reproduced from G. Herzer, *IEEE Trans. Mag.* **26**, 1397 (1990). Copyright 1990, with permission of IEEE

For *permanent nanomagnets* the archetype comes from a nanocomposite of $Nd_2Fe_{14}B$ grains of size 20–30 nm in a paramagnetic Nd- and B-rich matrix. Figure 4.10 illustrates the unit cell of $Nd_2Fe_{14}B$ which has the *c*-axis as the uniaxial anisotropy axis (Section 4.1.3). To be useful, a permanent magnet material requires a high remanence (M_r/M_s close to 1), a high coercive field and a high Curie temperature.

Nanocomposites are usually used to make working magnets. The nanocomposite is formed by taking rapidly solidified flake, or particles produced from flake, and then bonding with a filler (e.g., a polymer) or by forming diffusion bonds between particles or flakes by heat treatment under high pressure at elevated temperature. The route used to produce the final product may significantly affect the overall magnetic properties, as illustrated by Figure 4.11.

In the nanocomposite material there can be exchange coupling between grains, especially if the alloy is Fe-rich when bcc-Fe nanoparticles accumulate between the NdFeB grains, leading to remanence enhancement effects whereby the remanence can be increased significantly (Figure 4.12).

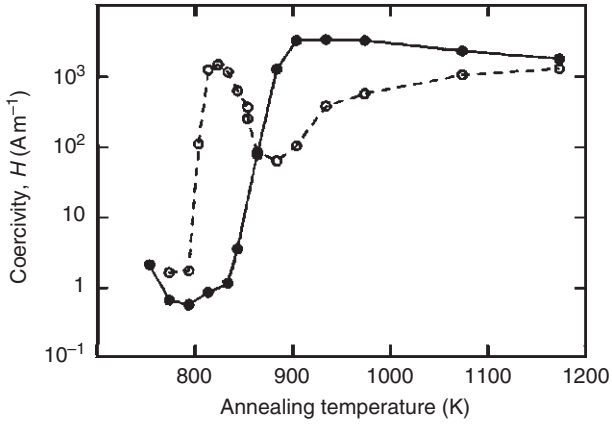

Figure 4.9 The variation of coercivity with annealing temperature in the FeCuNbSiB system. The open circles show the material without the crystal growth-retarding Nb present, whereas the closed circles correspond to the presence of a small amount (1 at%). The coercivity is significantly lower when the grain size is constrained by the Nb additive. Reproduced from G. Herzer, *IEEE Trans Mag*. **26**, 1397 (1990). Copyright 1990, with permission of IEEE

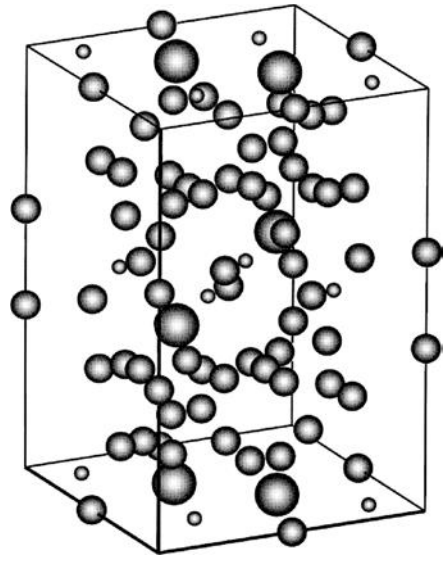

Figure 4.10 Tetragonal unit cell of $Nd_2Fe_{14}B$. The *c* axis (direction of uniaxial magnetic anisotropy) is vertical in this image

Figure 4.13 illustrates the importance of controlling the intergranular Fe thickness to ensure good exchange coupling between the $Nd_2Fe_{14}B$ grains. If the thickness of the Fe layer exceeds the exchange length, then coupling between NdFeB grains will be lost as the direction of magnetization in the Fe grain will rotate towards the intrinsic easy direction in the Fe crystal.

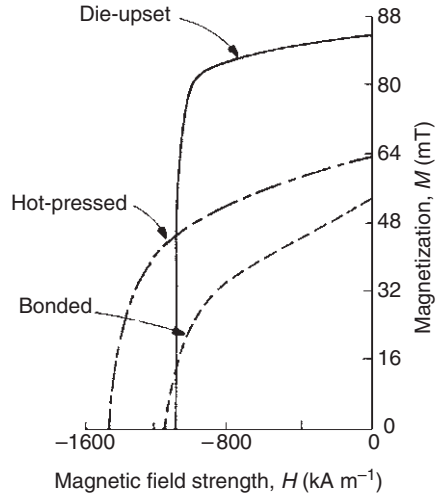

Figure 4.11 The effects of final magnet production on hysteresis loop shape in the second quadrant for NdFeB magnets. The die-upset nanocomposite involves forcing liquid metal into the die to minimize porosity. A hot-pressed nanocomposite magnet is a powder or flake consolidated under high temperature and pressure and the bonded nanocomposite is also a powder or flake treated with a binder, such as an epoxy resin. After R. C. O'Handley, *Modern Magnetic Materials: Principles and Applications*, Wiley, New York, 2000, p. 508

It is the continual development of alloy composition and control of physical nanostructure which has taken us very close to the theoretical limit for performance with the NdFeB family of magnets. Cordless power tools and miniature earphones on portable audio devices are just two current applications of such advanced nanomagnetic materials. Work is also in progress to produce high-efficiency electric motors for use in transportation. The energy product $(BH)_{max}$, is the parameter used to define the energy

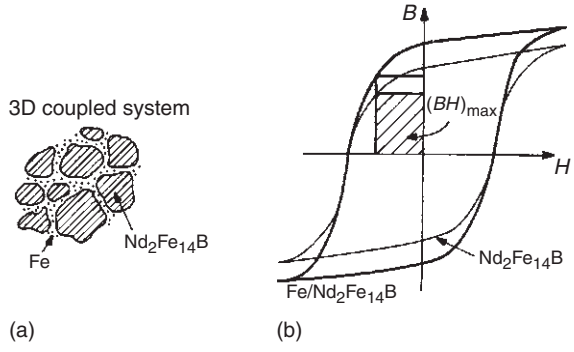

Figure 4.12 (a) A schematic diagram of the exchange-coupled alloy microstructure of $Nd_2Fe_{14}B$. (b) The corresponding hysteresis loop After R. C. O'Handley, *Modern Magnetic Materials: Principles and Applications*, Wiley, New York, 2000, p. 464. Copyright 2000, with permission of John Wiley & Sons, Inc.

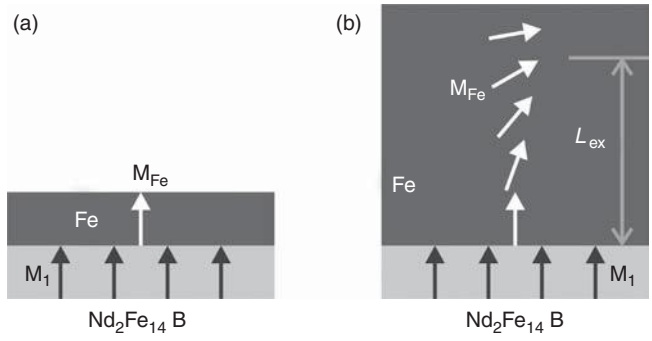

Figure 4.13 A schematic illustration of the effect of soft layer thickness on exchange coupling between grains in a permanent magnet nanocomposite. Black arrows represent the magnetization direction in the $Nd_2Fe_{14}B$ phase and white arrows represent the magnetization direction in the Fe layer. Redrawn after R. C. O'Handley, *Modern Magnetic Materials: Principles and Applications*, Wiley, New York, 2000, p. 465, Copyright 2000, with permission of John Wiley & Sons, Inc.

stored in an air gap in the magnet. This point is marked on Figure 4.12 for illustration. The highest value reported so far in an NdFeB type magnet is around $450\,kJ\,m^{-3}$.

Another system in this category is granular solids, produced when two immiscible species are co-deposited; e.g., FeCu or CoCu with 20–30% Fe or Co. A composite may be formed of nanomagnetic particles in a non-magnetic matrix. These materials may demonstrate giant magnetoresistance (Section 4.3.2) but high fields are usually needed to see maximum effect, and thus they are not best suited to devices.

The final system in this category is where a nanoparticulate magnetic film is grown on a suitable seeding layer. If the seed layer can be grown with a high crystallographic texture (close-packed direction) out of the plane, and with small grain size, then the functional overlayer can be both textured and nanostructured. Such films are candidates for recording media (Figure 4.14).

Modern recording media require small grain size to ensure low noise with many grains per bit. High coercivity is also essential so that the written information remains stable over time. If the grains can be magnetically decoupled, using non-magnetic grain

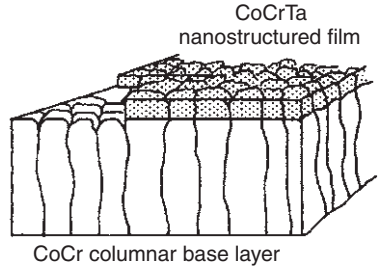

Figure 4.14 A schematic picture of a granular magnetic recording medium. In this example the crystallographic texture of the CoCr underlayer ensures that the functional CoCrTa layer has the necessary nanostructure. After R. C. O'Handley, *Modern Magnetic Materials: Principles and Applications*, Wiley, New York, 2000, p. 463. Copyright 2000, with permission of John Wiley & Sons Inc.

boundaries, stability against thermal erasure of information may also be increased. The growth of a suitably doped nanomagnetic layer on a columnar seed layer ensures these criteria are met. The doped grains are about 30 nm thick.

4.2.2 Geometrical nanomagnets

Self-assembly is developing as a very important technique in this area. One route to the production of nanomagnets comes from templating. Using lithographic techniques, a mask is formed which can be stamped in to a polymer resist. Then using lift-off or etching, a pattern of magnetic islands can remain. Alternatively, layered films may be directly lithographically patterned.

Block copolymer techniques (Chapter 8), or porous alumina, may be used to give a template in to which nanowires may be grown by electrodeposition. This whole subject area is still at the very early stages of exploration, but biological and data storage applications may come to rely on this new paradigm for the construction of smart magnetic materials.

If nanoparticles can be produced, then self-assembly by surfactant and ligand structuring can be used. This offers a number of advantages in that large areas might be covered by self-assembly, and the spacing between nanoparticles might be controlled by variation of the ligand lengths. There has been a recent report[1] of a self-assembled nanocomposite formed using FePt and Fe_3O_4 nanoparticles as precursors, giving an energy product of $160\,kJ\,m^{-3}$. This is already within a factor of three of the best NdFeB-type magnets. Thin film self-assembled permanent magnets have great potential for application in micro- and nanoelectromechanical systems (MEMS and NEMS) and also data storage.

Biomimetics can be employed, where the magnetic particles are carried in large molecules in an analogous way to haemoglobin in red blood corpuscles. The encapsulation of a magnetic nanoparticle in a protein, or other biocompatible shell, offers significant benefits for drug delivery and cancer therapy, as well as smart diagnostic systems.

It is worth noting that there have been geometrical permanent nanomagnet materials available for a number of years that rely on nanoscale geometrical effects for their properties. Alnico, an alloy of Fe with Ni, Co and Al additives, was first developed in 1938. There is an energetic preference for particle elongation along the $\langle 100 \rangle$ direction during production. This is driven by minimization of the magnetic charge density at the interface between particle and matrix. This can be practically realized by applying a field in a chosen direction during spinodal decomposition (a form of precipitation discussed briefly in Section 8.6.1). This leads to periodic (not sharp) composition fluctuations throughout the magnet volume.

It is shape anisotropy of the particles that produces the necessary anisotropy to produce hard magnetic properties in this instance. Figure 4.15 is a TEM micrograph showing the elongated particles in the matrix. The magnitude of shape anisotropy is not great, so the performance of the Alnico magnets is not as impressive as of the NdFeB magnets discussed above.

[1] H. Zeng, J. Li, J. P. Liu, Z. L. Wang and S. Sun, *Nature*, **420**, 395 (2002).

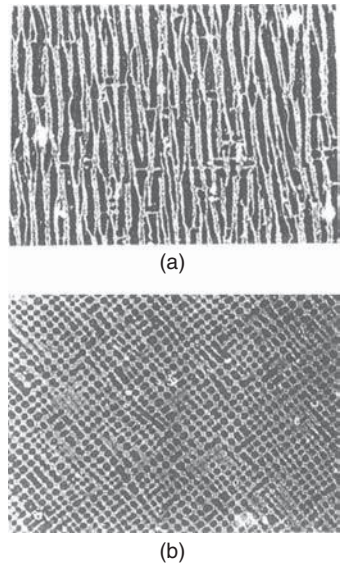

Figure 4.15 The nanostructure of Alnico 8 after isothermal heat treatment in a magnetic field for 9 h at 800 °C: (a) view perpendicular to the direction of the applied field, (b) view along the direction of the applied field. The microstructure has a periodicity of approximately 32 nm. After R. C. O'Handley, *Modern Magnetic Materials: Principles and Applications*, Wiley, New York, 2000, p. 481

The final category is layered magnets, where one dimension is in the nanometre range. It is in this category where effects at surfaces and interfaces have been observed. For example, there is growing evidence that in chemically homogeneous films with thickness less than 20 nm, the magnetoelastic coefficients are markedly different to the bulk. This is most clearly illustrated in data from our own work on $Ni_{81}Fe_{19}$ plotted in Figure 4.16, where the composition has been chosen for zero magnetostriction *in the*

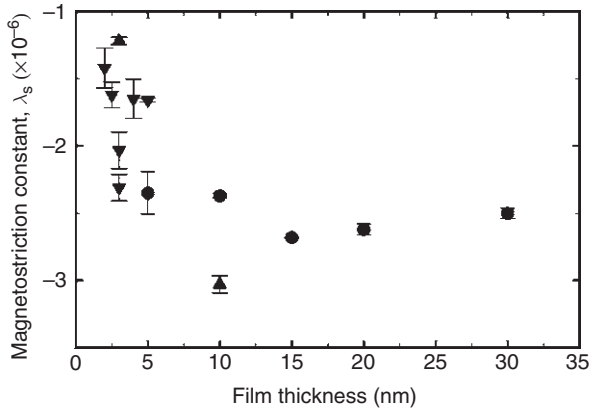

Figure 4.16 Plot of magnetostriction constant λ_S against film thickness for NiFe on SiO_2. The different symbols refer to different data sets. Data courtesy of M. P. Hollingworth

bulk. There are major implications for such devices as spin valves, where the soft magnetic layers are 'buried' in a stack of many layers. This is inevitably going to place the layers under strain.

The reduced symmetry at a surface or interface (atoms only coordinated over a hemisphere) can lead to changes in magnetic anisotropy. As films (or particles) decrease in dimension, surface effects may dominate volume effects.

4.3 MAGNETORESISTANCE

4.3.1 Contributions to resistivity in metals

The basic electronic properties of solids are covered in Chapters 1 and 3 and the reader may need to refer to these for background. We outline here the basis of Drude theory, which assumes that the mean free path λ between electron scattering events is very much longer than the lattice spacing. The incremental velocity δv acquired by an electron in the direction of an electric field E in time τ is given by

$$\delta v = \frac{eE\tau}{m^*}. \tag{4.28}$$

This gives a conductivity σ of

$$\sigma = \frac{ne^2\tau}{m^*} = \frac{ne^2\lambda}{\hbar k_F}, \tag{4.29}$$

where n is the electron density and k_F is the wavevector at the Fermi level. The finite mean free path arises from the presence of defects, phonons, magnetic fluctuations and occasionally electron–electron scattering.

In the effective mass approximation $E_k = \hbar^2 k^2/2m^*$ where m^* is close to the electron mass except when k is close to the edge of the Brillouin zone where the electron is Bragg reflected. The Brillouin zone of a crystal with N unit cells contains Nk points, so a full zone can hold $2N$ electrons (counting electron spin). Hence if the number of electrons per atom is less than or equal to order unity then the electrons behave like free electrons.

The s electrons behave as almost free electrons, so an s electron carries the current efficiently; any scattering off impurities is weak. The overall effect of all the atom cores is very weak (the electrons are free) and if an atom is displaced as in a phonon, it produces very little scattering. The band and density of states pictures make it clear that the *only* electron states that matter are those at the Fermi level.

Electron bands for d orbitals are much narrower than those for s electrons, so m^* will be higher. Also if the band is narrow, then the electrons will interact much more strongly with the lattice than for a wide free electron band. This means that they are much more affected by any imperfections, so that we expect that τ will be much shorter for d electrons than for s electrons. Hence we should expect d electrons to contribute less than s electrons to the conductivity σ, even though there are more of them. In fact, d electrons seriously impede the s electrons. However, there is an alternative view, where

hybridization occurs (mixing of s and d states – see Section 6.1.2.1 for more details) and we should think of conduction by the hybridized bands. These have mostly d character, hence they have high effective mass and so conduct badly.

From Fermi's golden rule we find that the probability of scattering depends on the number of available states, which is the density of states at the Fermi surface. Thus we see that the s electrons have a greatly reduced lifetime, τ, when there are available d states for scattering.

In copper the s electrons carry the current efficiently and any scattering off impurities is weak; the s electrons are behaving as almost free electrons. There are also very few states for an electron to scatter into because the density of states is so low. If it is scattered, it stays an s electron and so continues to contribute to the conductivity.

In a transition metal the s electrons scatter readily into d electron states because there are so many available states. The d electrons have a very short scattering time and a large effective mass and so they do not contribute to the conductivity. The result of this is surprising; some electron states at the Fermi level are needed for conductivity.

In order to see significant spin-dependent transport effects in ferromagnets, two criteria must be satisfied. There must be different conductivities for electrons in the majority (spin-up) and minority (spin-down) spin bands, and little spin mixing so that the two channels act independently.

Spin flip (sf) scattering occurs because of the spin–orbit interaction and also because of the scattering of the electrons by the spin waves, which makes spin flip scattering temperature dependent. An electron must change its spin and its wave vector (spatial wavefunction) simultaneously. This is a weak effect because the spin–orbit interaction energy is much less than the Coulomb interaction energy. We expect that an electron will undergo N spin-conserving scatterings before it flips its spin. N is a large number and temperature dependent. We can write $\tau_{\mathrm{sf}} = N\tau_0$.

In order to make a device, we need to know how far an electron travels before a spin flip occurs. Because of scattering, the electron is travelling in a random walk as it is scattering N times. So we need to consider the distance travelled in a random walk, $\langle \mathrm{R}^2 \rangle^{1/2}$:

$$\left\langle R^2 \right\rangle^{1/2} = \mathrm{N}^{1/2}\lambda = \tau_0 v_{\mathrm{F}} \sqrt{\frac{\tau_{\mathrm{sf}}}{\tau_0}} = v_{\mathrm{F}} \sqrt{\tau_0 \tau_{\mathrm{sf}}}. \tag{4.30}$$

Spin flip scattering is usually ignored, which means that we consider the conductivity in a ferromagnet in terms of two independent spin channels conducting in parallel. The total current density is given by $I = j_\uparrow + j_\downarrow$, and the voltage drop across the devices is $V = \sigma_\uparrow j_\uparrow = \sigma_\downarrow j_\downarrow$. Here j is the current density in either the spin-up or spin-down channel. We are now able to consider the effects of magnetic fields on electron transport.

4.3.2 Giant magnetoresistance

With the advent of nanomagnetic materials in the form of granular solids or multilayers (Section 4.2) there are now systems that demonstrate very significant spin flip scattering. Giant magnetoresistance (GMR) is a generic term applied to a range of phenomena

where there is a significant (>5%) change in electrical resistivity as the sample magnetization magnitude or direction is varied.

We can consider a number of features in a study of GMR. Firstly, the structure demonstrating GMR is usually a combination of normal metal and ferromagnetic layers. The electrical conductivity depends on the relative orientation of magnetization in successive ferromagnetic layers in the stack. Switching the relative magnetization of the layers from parallel to antiparallel defines two states, high and low resistivity, respectively. In terms of sensor technology, these two states are easily discriminated and may be ascribed to the binary states 0 and 1. This has opened up the possibility of applications in data storage technology (see below).

Two geometries are commonly used in GMR studies. The current may flow in the plane of the layers (CIP) or current perpendicular to the plane of the layers (CPP). These are shown schematically in Figure 4.17. As the layers are only a few nanometres thick in each case, the CIP geometry offers high resistance from the small cross-sectional area, and the attendant voltages are easy to measure. To make CPP measurements tractable, lithography must be used to create pillars of small cross-sectional area to achieve voltages suitable for detection.

To satisfy the criteria developed above for spin-dependent scattering, the lateral dimensions must be small compared with the electron mean free path. Hence each electron samples different layers and/or directions of magnetization between scattering events.

A simple model may be developed based on resistor networks. In a ferromagnet there are two different resistances for the two spin channels: $\rho_{\downarrow}$ for the minority spin electrons

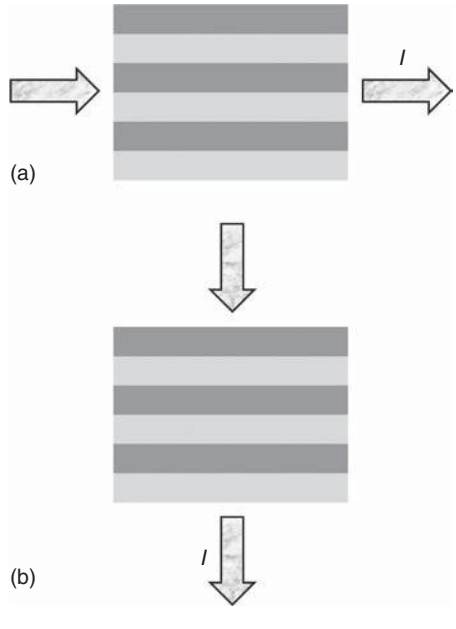

Figure 4.17 The two geometries used in GMR studies: (a) CIP in plane and (b) CPP current perpendicular to plane

and $\rho_\uparrow$ for the majority spin electrons. The resistivity of the non-magnetic metal will be independent of the spin and is designated ρ_0.

We take the thicknesses of the ferromagnetic layers to be t_F and the thickness of the spacer layer to be t_s. Consider the resistance in CPP for two ferromagnetic layers aligned with magnetizations parallel separated by a non-magnetic spacer. We take A as the planar area of the multilayer stack. For two ferromagnetic layers separated by a single non-magnetic conductor, we can use a simple resistor model again.

The total resistivity for the spin-up electrons is $R_\uparrow = 2t_F\rho_\uparrow + t_s\rho_0$. The total resistivity for the spin-down electrons is $R_\downarrow = 2t_F\rho_\downarrow + t_s\rho_0$. The net resistance for the two conduction paths is obtained by adding the two spin contributions in parallel:

$$\frac{1}{R_{\uparrow\uparrow}} = \frac{1}{R_\uparrow} + \frac{1}{R_\downarrow} = \frac{2t_F(\rho_\uparrow + \rho_\downarrow) + 2t_s\rho_0}{(2t_F\rho_\uparrow + t_s\rho_0)(2t_F\rho_\downarrow + t_s\rho_0)}. \tag{4.31}$$

The same considerations apply for two ferromagnets aligned antiparallel. In the parallel case each spin is a minority spin in one ferromagnetic region and a majority spin in the other. The resistances are equal, so

$$R_\uparrow = R_\downarrow = t_F\left(\rho_\uparrow + \rho_\downarrow\right) + t_s\rho_0, \tag{4.32}$$

giving $R_{\uparrow\downarrow} = R_\uparrow/2$ (again by conductors in parallel). The GMR ratio is commonly defined as $(R_{\downarrow\uparrow} - R_{\uparrow\uparrow})/R_{\uparrow\uparrow}$.

The resistance is always larger for the antiparallel alignment (both species of electron must pass through the region of high resistance) and lower for parallel alignment as one species of electron 'shorts out' the other). Hence GMR is always positive and can be very large.

Writing $\alpha^+ = \rho_\uparrow/\rho_0$ and $\alpha^- = \rho_\downarrow/\rho_0$, we have:

$$\mathrm{GMR} = \frac{(\alpha^+ - \alpha^-)^2}{4\left(\alpha^+ + \dfrac{t_F}{2t_s}\right)\left(\alpha^- + \dfrac{t_F}{2t_s}\right)}. \tag{4.33}$$

The effect is bigger if the contribution to the resistance from the spacer is small.

It is straightforward to include any boundary resistance by redefining the thickness of the ferromagnetic layer to take account of it. We write $t_F\rho_\uparrow + r_j = t_F^j\rho_\uparrow$ and similarly for the minority electron, which gives the modified result

$$\mathrm{GMR} = \frac{(\alpha^+ - \alpha^-)^2}{4\left(\alpha^+ + \dfrac{t_F^j}{2t_s}\right)\left(\alpha^- + \dfrac{t_F^n}{2t_s}\right)}, \tag{4.34}$$

where r_j is the junction resistance. The model is not exact. There is still much dispute concerning the details, and it is believed that electron interference effects give small deviations from the simple model.

There are two basic reasons why there is GMR. Firstly, the resistivities for the majority and minority electrons are different, as discussed above. There is also likely to be scattering and reflection at the interfaces. If the interfaces are rough, this will increase the amount of scattering. As the electrons enter the ferromagnetic layer, the scattering depends on the density of states for the spin-up and spin-down electrons.

The second reason is due to interface resistance. The probability of reflection of a wave from one medium to another (R) where the wavenumbers are k and k' is

$$R = \left|\frac{k - k'}{k + k'}\right|^2.$$

This means that the probability of reflection vanishes if the wavenumbers are very similar in the layers at either side of the boundary, and is large if they are very different. It has been shown that there is a nearly perfect match between the wavevector for spin-up electrons in Co, and the wavevector of free electrons in Cu. There is a poor match between the wave vector of spin-down electrons in Co and the wave vector of free electrons in Cu. Hence most of the spin-down electrons will be reflected while the spin-up electrons will pass straight through the boundary. The reverse effect is seen for Fe/Cr, so it is the minority electrons which pass through.

We shall now consider the constraints that are placed on the dimensions of the layer thicknesses for GMR to occur. If the spin flip scattering may be neglected, the spin currents are conserved. In CIP geometry the mean free path in the normal metal must be less than the spin flip scattering length. At any boundary, in equilibrium, $\mathbf{j} \cdot \hat{\mathbf{n}} = 0$ ($\hat{\mathbf{n}}$ is the unit vector normal to the boundary) is continuous (because $\nabla \cdot \mathbf{j} = 0$ from Maxwell's equations), hence in a CPP structure the important requirement is that the total thickness of the device is less than λ_{sf}, the spin diffusion length.

For CIP we consider two cases: layer thickness large or small compared with the scattering length between collisions, λ_o. It is the shortest such length that matters. For small spacings, we take an average resistance over the whole sample; that is, no Ohm's law behaviour for each component. For large spacings, we take separate Ohm's law behaviour for each component. The current flow is in the material with the low resistance (the spacer). Electrons do not travel much between different components, and the GMR vanishes.

The resistance of a few monolayers of transition metal is extremely small. Almost all GMR experiments are done using a CIP geometry. A superconducting circuit is needed to detect CPP unless lithographic patterning is used to reduce the effective area.

Consider a multilayer made of layers of Co (n Å) and of Cu (m Å) with N repeats. (1 Å $= 10^{-10}$ m). The interatomic spacings in Co and Cu are both $\sim$2.5 Å, so the multilayers are made with only a few atomic planes. This is written as [Co(n Å)/Cu(m Å)]$_N$. The exchange interaction between Co layers oscillates with the thickness of the spacer layer. It may be assumed that the spacing has been chosen so that the interaction is antiferromagnetic, and the magnetizations of the two layers are taken as M_A and M_C.

Now assume that we have a magnetic field B acting. The energy per unit area will be

$$U = -JM_AM_C - Bt_{Co}(M_A - M_C). \tag{4.35}$$

The net field on the C layer changes sign when $B = JM_A/t_{Co}$ and the magnetization of the C layer flips round. The resistivity changes from that appropriate for an

antiferromagnetic structure to that for a ferromagnetic structure. Figure 4.18 shows resistance with magnetic field for an Fe/Cr multilayer. The saturation field, H_s, can be used to deduce the exchange from the above theory. In this diagram $R_{\uparrow\downarrow}$ is the same as $R(H = 0)$ and $R_{\uparrow\uparrow}$ is equal to $R(H > H_s)$.

Figure 4.19 shows the variation of saturation field H_s for an NiFe/Ru multilayer as a function of the ruthenium layer thickness. The regions where the exchange is ferromagnetic correspond to the minima in the saturation field.

As described in Section 4.2.1, we can consider a granular alloy for GMR containing small, usually irregular grains of a ferromagnet in a non-magnetic matrix. In the absence

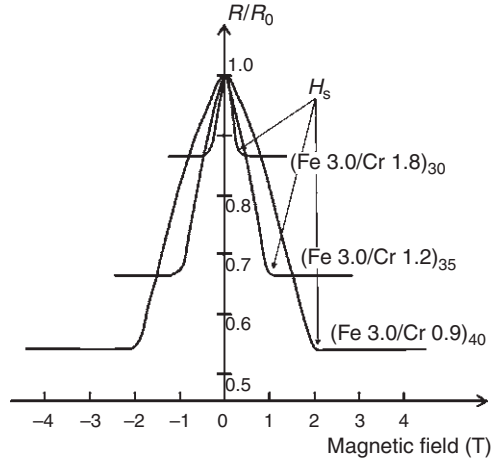

Figure 4.18 Normalized resistance (R/R_0) as a function of applied magnetic field for an Fe/Cr multilayer. The notation (Fe x/Cr y)$_z$ denotes a stack of z bilayers of x nm of iron and y nm of chromium. H_S is the saturation field as defined in the text. Redrawn with permission after B. Heinrich and J. A. C. Bland, *Ultrathin Magnetic Structures*, Vol. I, Springer-Verlag, Berlin, 1994, p. 98. Copyright 1994 Springer-Verlag

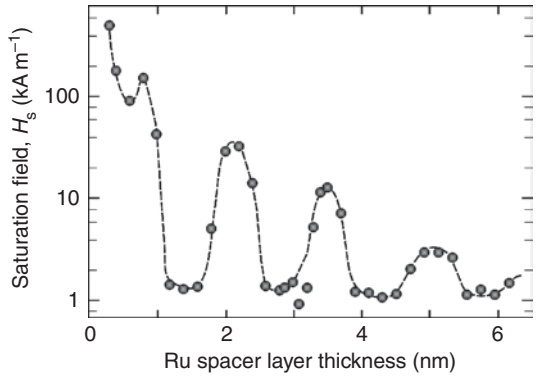

Figure 4.19 Dependence of saturation field on Ru spacer layer thickness in an NiFe/Ru multilayer at room temperature. Redrawn with permission after B. Heinrich and J. A. C. Bland, *Ultrathin Magnetic Structures*, Vol. I, Springer-Verlag, Berlin, 1994, p. 161. Copyright 1994 Springer-Verlag

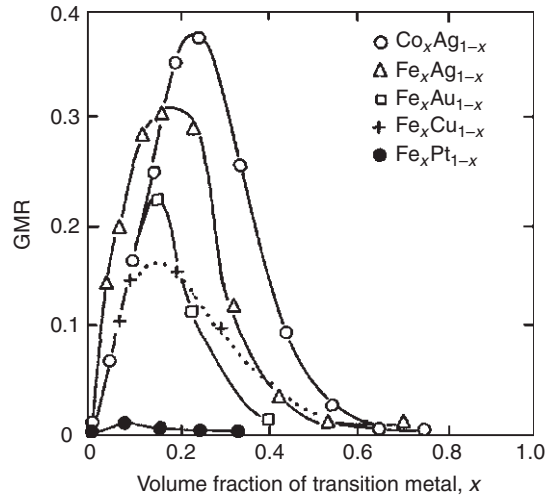

Figure 4.20 Variation of GMR with volume fraction of magnetic components. For several transition metal–noble metal granular systems. After R. C. O'Handley, *Modern Magnetic Materials: Principles and Applications*, Wiley, New York, 2000, p. 594. Copyright 2000 with permission of John Wiley & Sons Inc.

of an applied field, the grains are randomly arranged due to their own shape anisotropy and a long-range exchange (RKKY) interaction between them.[2] An applied field lines up the grains.

Provided that the electron mean free path is larger than the spacing between the ferromagnetic granules, the resistance will drop in the aligned state. Transition metal (e.g., iron) and noble metal (e.g., silver) systems show this GMR. Figure 4.20 shows some data for transition and noble metal composites.

4.3.3 Spin valves

In applications such as data storage there is a requirement for a sensor that converts a changing magnetic field into a changing voltage. The changing field is derived from the stray field from a recording medium such as a hard disk or tape. The voltage, which needs to be linearly related to the stray field direction and/or magnitude, is used as the read signal and is transposed into audio or digital signals for interpretation.

To create a hard disk drive reader, one must have a device that responds at very high frequencies to very low magnetic fields. The high frequencies are necessary in order to have high rates of data transfer. One such device, derived from the basic GMR physics set out above, is the spin valve. This is a device with only two ferromagnetic layers. One layer is pinned; its direction of magnetization being unperturbed by the changes in field that are to be detected. The other layer, called the free layer, is sensitive to the stray

[2] See R. C. O'Handley, *Modern Magnetic Materials: principles and applications* (Wiley, NewYork 2000) for a full discussion.

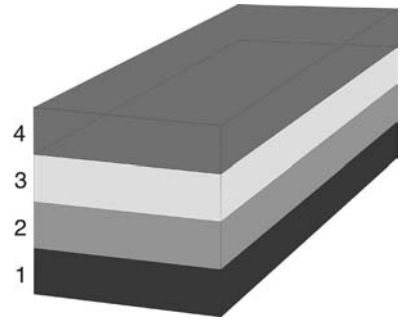

Figure 4.21 A schematic diagram of the structure of a spin valve. Layer 1 is the antiferromagnetic layer (e.g. FeMn) and layer 2 is the pinned soft magnetic layer (e.g., NiFe). A copper spacer layer, layer 3, separates the lower two layers from a free soft magnetic layer, layer 4 (e.g., NiFe).

fields; that is, the direction of magnetization in the free layer may be reversed by the stray fields. Permalloy, an alloy of Ni and Fe, is usually chosen for both layers. The chosen alloy has a very low coercive field and anisotropy field (but note the discussion in Section 4.2.2) and is a strong ferromagnet, so it has a good GMR response. The pinned layer is also NiFe and has a direction of magnetization defined by exchange or anisotropy bias (Section 4.3.4) from an adjacent antiferromagnetic layer; e.g., IrMn or FeMn.

The pinned layer is magnetized in-plane as it is prepared in such a way as to have uniaxial in-plane anisotropy. The structure is cooled down through the ordering temperature of the antiferromagnet in an external applied field (Section 4.3.4).

The spacer, usually Cu or Ru, is chosen so as to give the smallest possible magnetic coupling between the two ferromagnetic layers.

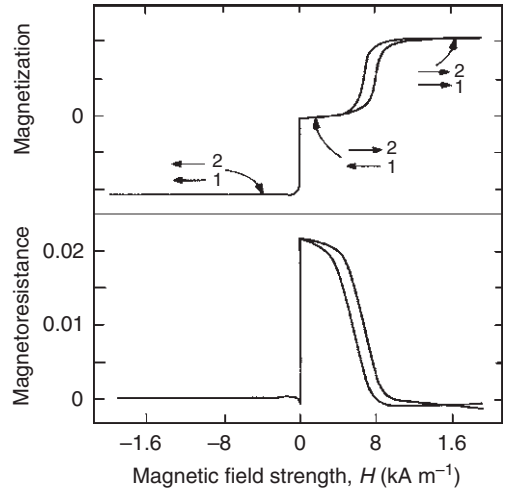

Figure 4.22 The magnetization and magnetoresistance curves for a spin valve. The arrows indicate the magnetization direction in the two ferromagnetic layers. After R. C. O'Handley, *Modern Magnetic Materials: Principles and Applications*, Wiley, New York, 2000, p. 596. Copyright 2000, with permission of John Wiley & Sons Inc.

Figures 4.21 and 4.22 illustrate the principles of the spin valve. The magnetic layers are NiFe or CoFe alloys. For all applied fields that are negative, the pinned and free layer magnetizations represented by the arrows in Figure 4.22 are parallel and the device is in a low-resistance state. As the applied stray field becomes sufficiently positive, the free layer may rotate, reducing the net magnetization to zero and causing an almost stepwise increase in the resistance. Further increases of stray field in the same sense will eventually cause the pinned layer to rotate, returning the device to a low-resistance state. A practical device would only operate for small field excursions around $H = 0$, leaving the pinned layer unchanged. It is simple to see that the two resistance states may be ascribed the logical states 0 and 1. The changes in state are detected in terms of the voltage change across the spin valve for a constant current flowing through the device.

A full understanding of the microscopic origins of exchange bias remains to be found, but many current disk drive systems are now using spin-valve technology for the read head.

4.3.4 Tunnelling magnetoresistance

Whilst spin valves are already developed sufficiently to be in production, research work continues on another form of magnetoresistive device that relies on electron tunnelling through an oxide barrier between two ferromagnets. This results in tunnelling magnetoresistance (TMR).

Consider two ferromagnets separated by an insulating tunnel barrier. Electrons may tunnel across the barrier, preserving spin provided the spin flip scattering length is greater than the barrier width. Hence the resistance across the barrier will be much lower if there is a large density of states available for the tunnelling electrons on both sides of the barrier.

We now look at the densities of states on both sides of a tunnelling barrier for both spin components. We consider the parallel configuration; that is, the magnetizations parallel across the barrier. There will be a small amount of tunnelling across the barrier. For the parallel magnetization we have a large density of states tunnelling to a large density of states.

Early experiments in the manganites (oxide materials based on compounds such as LaCaMnO) showed that when the material was granular, rather than composed of large single crystals, there was a very large magnetoresistance at low temperatures that occurred for small magnetic fields. It was realised that this occurred because of tunnelling between the grains through the resistive material at the grain boundaries. One of the features of the grain boundary is that the exchange paths are broken. This means that very small fields are required to change the relative orientation of the two grains.

More recently structures have been made where an insulating layer is grown as a tunnel barrier between two ferromagnets. The insulator must be very thin, usually only a few lattice spacings. This is because the total probability of tunnelling is proportional to $\exp(-2d/\lambda)$, where d is the thickness of the tunnel barrier and λ is the decay length of the electron wavefunctions in the barrier. If the barrier is not perfect, then pinholes may appear which do not show the desired magnetoresistance.

In a TMR device the requirement is for one free layer and one pinned layer, as in a spin valve (Figure 4.21). One of the common ways to fabricate an insulating layer is to grow a layer of Al and then oxidize it to Al_2O_3. The quality of the device is lowered if there is an unreacted layer of Al, but on the other hand allowing too much oxidation so that transition metal oxides like CoO are formed is counterproductive because such

oxides are antiferromagnetic and hence destroy the spin polarization. There is an asymmetry between the magnetic layers. One is grown on the substrate and is a high-quality epitaxial layer and the other is grown on top of the amorphous Al_2O_3. In most cases the layer that is magnetically soft is the one that is underneath the Al_2O_3 and was grown directly on the substrate.

Most of the tunnel junctions that are being developed for current applications are based on transition metals. Co is often used as it has a high spin polarization and it is combined with NiFe or FeCo as the soft layer. Figure 4.23 shows magnetoresistance data for a $Co/Al_2O_3/CoFe$ TMR device. The form of this data may be taken as generic for all tunnel junctions.

The advantages of using transition metals is the high transition temperatures, leading to robust devices at room temperature, and the ease of fabrication, similar to that for GMR spin valves.

Another possibility is hybrid devices in which an oxide is combined with a transition metal. These appear to be very promising as they combine the very large TMR expected for an oxide with the good performance at room temperature.

Although the ideas of TMR and GMR spin valves appear similar, there are many very important differences that result in replacing the metallic non-magnetic layer with an insulating layer. The first and most obvious experimental difference is that the overall resistance of the device is now much higher. Whereas it is very difficult to carry out GMR experiments in the current perpendicular to the plane geometry, as the resistances are too small to measure, it is absolutely impossible to perform TMR in anything other than the CPP geometry; no current at all will cross the barrier unless it is

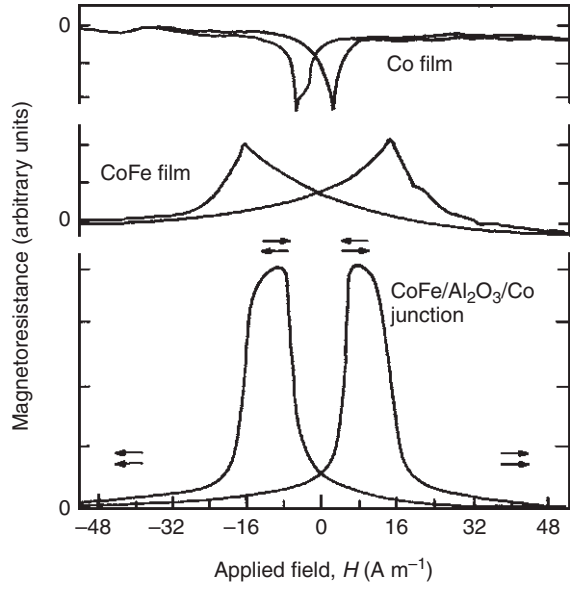

Figure 4.23 Anisotropic magnetoresistance in each individual CoFe and Co electrode and the junction magnetoresistance in $CoFe/Al_2O_3/Co$ spin tunnel junction versus applied field. After R. C. O'Handley, *Modern Magnetic Materials: Principles and Applications*, Wiley, New York, 2000, p. 607. Copyright 2000 with permission of John Wiley & Sons Inc.

driven by a voltage. In GMR the current is carried predominantly by the majority electrons that have a low density of states, hence a longer mean free path. In TMR the simple theory indicates that the effect depends only on the density of states. In fact there have been a number of experiments that have shown that this is not correct and that the way in which the mobile electron wavefunctions can match onto the empty conduction band states in the barrier is also a factor.

In GMR spin valves, one must choose a metal spacer layer that gives a very small exchange coupling between the magnetic layers. This is important if the device is to respond to low switching fields. This is not an issue in tunnel devices as the magnetic interactions do not easily cross an insulating layer. However, it is hard to ensure that one of the layers is really magnetically soft when there is a possibility of oxide formation and strain due to the amorphous layer.

The TMR junctions are particularly good candidates for magnetic random access memory (MRAM). This is because the two layers are not coupled magnetically, so the junction will stay almost indefinitely in one configuration. Another very attractive possibility is that the tunnel junctions will be used in three-terminal devices to make spin transistors, as well as other aspects of spin electronics, or spintronics. Spintronics is still in its infancy and it is impossible to foresee which directions will prove the most attractive.

4.4 PROBING NANOMAGNETIC MATERIALS

The power of the electron microscope has been amply discussed in Chapter 2. For nanomagnetic materials it is the use of scanning probe techniques, and in particular magnetic force microscopy, which is important.

A magnetic force microscope (MFM) is essentially the same as an atomic force microscope (AFM). However, the scanning probe is coated with a layer of magnetic material, which may be magnetically hard (e.g., CoCr) or magnetically soft (amorphous ferromagnetic alloy; e.g., FeBSiC); a tip is shown in Figure 4.24. It is usual to take a line scan in contact mode to give the topographic information, and then rescan the line at a fixed flying height of a few tens of nanometres to obtain the magnetic contrast. In contact mode van der Waals forces, which have a much shorter range than the magnetic forces, dominate and only topography is seen. At the flying height, the longer-range

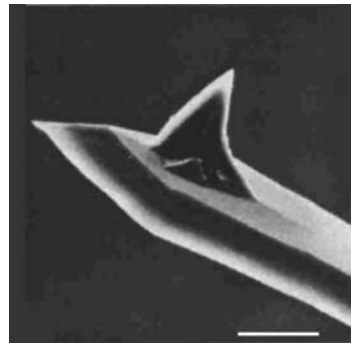

Figure 4.24 Scanning electron microscope image of an MFM-coated tip. The scale bar is 10 μm

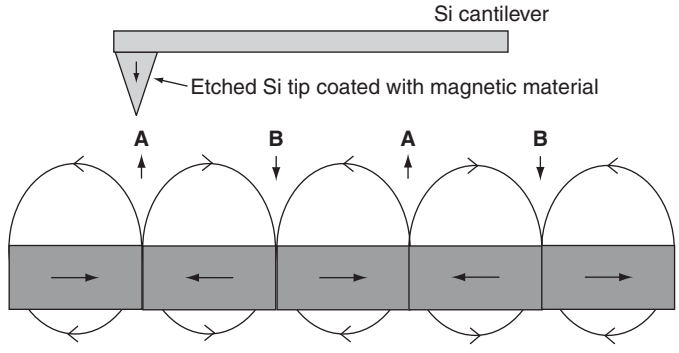

Figure 4.25 A schematic of the principle of MFM. The sample is magnetized in-plane, giving rise to stray fields above the plane vertically upwards (A) and vertically downwards (B). The tip is shown magnetized downwards, so it will see repulsion at A and attraction at B. Magnetic field lines are indicated by arrows

magnetic interactions between the tip dipole moment and the stray field from the sample are detected (Figure 4.25).

An oscillating cantilever (typically 70 kHz) would typically be used for high sensitivity. The tip is sensitive to the force gradient $\partial F_z/\partial z$, which modifies the effective cantilever spring constant k_{eff}: this produces a change in angular frequency

$$\omega_0 = \sqrt{\frac{k_{\text{eff}} - \partial F_z/\partial z}{m_{\text{e}}}} \tag{4.36}$$

where m_e is the mass of the cantilever. If, as is usual, $\partial F_z/\partial z \ll k_{\text{eff}}$ then we can write:

$$\omega' = \omega_0\left(1 - \frac{\partial F_z/\partial z}{2k_{\text{eff}}}\right) \quad \text{so} \quad \Delta\omega = \omega' - \omega_0 \approx -\frac{\omega_0}{2k_{\text{eff}}}\frac{\partial F_z}{\partial z}. \tag{4.37}$$

For an attractive force there is a decrease in resonance frequency, and vice versa; this change is used to generate the contrast. As an example, Figure 4.26 shows data from a

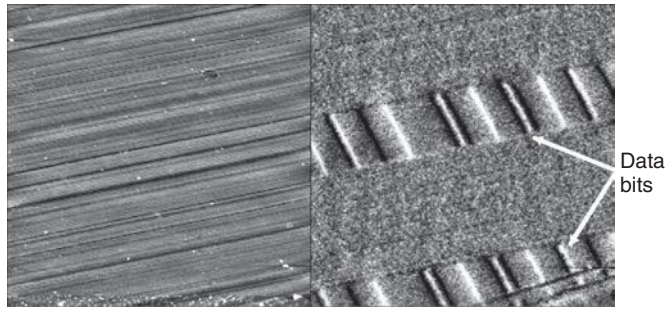

Figure 4.26 AFM/MFM image pair taken on a hard disk. The 'black' data bits, visible in the MFM tracks, are where there is an attractive force between head and disk, and the 'white' data bits are where the force is repulsive. The images are of an area having side 18 μm, and the height scale on the AFM image is up to 100 nm (lightest regions). Image courtesy of Dr M. Al-Khafaji, University of Sheffield

simultaneous AFM and MFM experiment on a magnetic storage disk. The AFM image shows the scratches that come from the disk polishing process. These do not appear in the MFM image, but instead we can see the tracks and data bits (single bits, dibits and tribits).

4.5 NANOMAGNETISM IN TECHNOLOGY

Figure 4.27 shows a standard PC hard disk drive. Inside this particular drive there are two hard disks, coated on each side, and four read/write heads on the flyer. Currently (2004) you can buy drives offering capacities greater than 400 Gbyte for a desktop PC. As the data storage density increases, so the physical size of each bit (1 or 0) decreases. In order to read/write, the head must be capable of interacting with a smaller and smaller volume, and sensing a smaller and smaller absolute field value. e.g., at 10 Gbit/in^2 (1.6 Gbit/cm^2) each bit is less than 1 μm square. This also requires the head to get closer to the disk surface (currently the head travels a mere 12 nm above the disk surface). It is analogous to

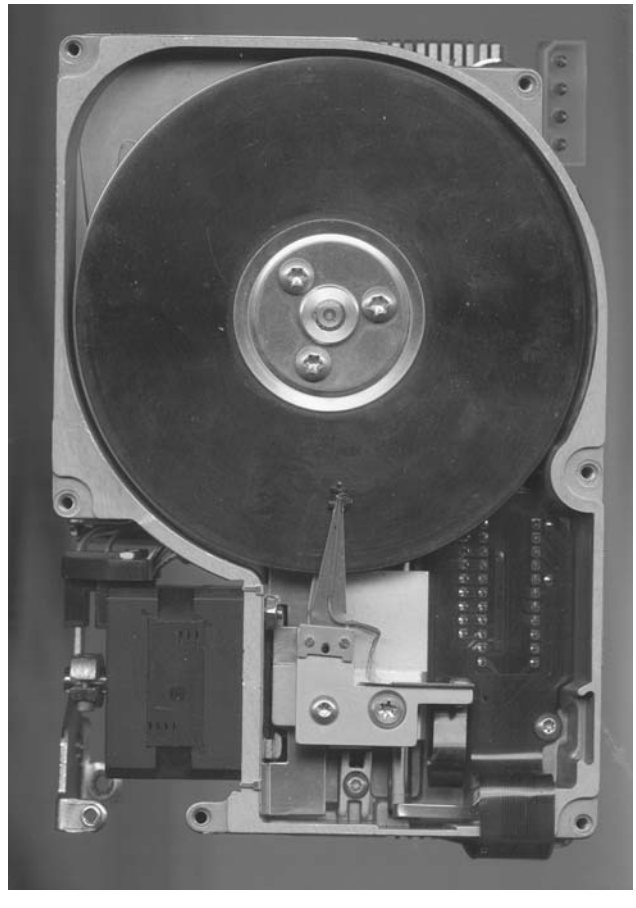

Figure 4.27 The inside of a computer hard disk drive

Figure 4.28 The all-electric go-kart. Photo courtesy of Professor D. Howe, University of Sheffield

flying a Boeing 747 on full throttle (800 kph) 3 m above the ground and following the land contours! Spin-valve heads have now been introduced, and may be followed by TMR devices as discussed above. Methods of self-assembly may be used to increase the areal density of information stored on the disk surface. The challenge remains to keep to the demand anticipated in the road map shown in Figure 4.1.

It has only been possible to develop personal entertainment systems such as the Sony Walkman because of extensive research on nanomagnetic materials. The miniature, high-fidelity ear phones use NdFeB permanent magnets to give audio power at low battery drain and in a small volume. The motor to turn the cassette tape or the CD is also less energy intensive with the fitting of NdFeB magnets. This gives prolonged battery life. Developments in soft magnetic materials have allowed the production of more sensitive analogue heads for interrogating the tape, again requiring less battery drain.

The cordless screwdriver or power drill can deliver a torque beyond the capability of most home decorators. Again it is high-efficiency NdFeB-based motors that give the advantage in terms of power and battery life. There are also extensive programmes to use nanomagnetic materials in new forms of electric traction. Figure 4.28 shows an all-electric go-kart developed by a team in Sheffield. There is a motor in each wheel hub, with NdFeB magnets offering the power and efficiency gain.

4.6 THE CHALLENGES FACING NANOMAGNETISM

The grain size of magnetic particles cannot be reduced indefinitely without affecting the magnetic properties. Below a certain critical size the remanent magnetization is no

longer fixed in direction by anisotropy, but can be flipped by thermal energy. If P is the probability of switching, then

$$P \propto \exp\left(\frac{-VK_u}{k_B T}\right), \tag{4.38}$$

where K_u is the local uniaxial anisotropy in the grain of volume V. The superparamagnetic radii for stability are typically 7 nm for 1 year's lifetime and 6 nm for 1s lifetime, for $K_u = 10^5\ Jm^{-1}$. This limits the simple option of increasing recording density by decreasing the size of particles currently used to coat disks. Materials of ever increasing anisotropy constant such as FePt and CoPt are under investigation, but eventually there will have to be a move towards lithography or self-assembly.

For extensive use of spintronics, there are processing compatibility issues between CMOS (complementary metal oxide semiconductor) electronics and metals, which will have to be resolved. The physics of magnetism and electron transport at interfaces must also be investigated further to resolve issues of spin flip and uncontrolled anisotropies at interfaces.

It is even fair to say that nanomagnetism faces the challenge of being in some senses already well developed. Alnico and NdFeB magnets have been around for a number of years and are already in applications at the low-cost, high-volume end of the market. Other nanotechnologies need to catch up.

Given the progress over the past 20 years, it would be a brave person who would go further in forecasting the impact of nanomagnetism on industry and commerce, but it will remain an integral part of many systems for years to come.

BIBLIOGRAPHY

General background

R. M. Bozorth, *Ferromagnetism*, IEEE Press, New York, 1993.
B. D. Cullity, *Introduction to Magnetic Materials*, Addison-Wesley, Reading MA, 1972.
D. Craik, *Magnetism: Principles and Applications*, John Wiley & Sons, Inc., New York, 1995.
R. C. O'Handley, *Modern Magnetic Materials: Principles and Applications* John Wiley & Sons, Inc., New York, 2000.
B. Heinrich and J. A. C. Bland (eds), *Ultrathin Magnetic Structures*, Vols I and II, Springer-Verlag, Berlin, 1994.
R. Skomski and J. M. D. Coey, *Permanent Magnetism*, IoP Publishing, Bristol, 1999.
S. Blundell, *Magnetism in Condensed Matter* Oxford University Press, Oxford, 2001.

Nanomagnetism

H. S. Nalwa, *Magnetic Nanostructures* American Scientific Publishers, Los Angeles, 2002.
A. Hernando, *Nanomagnetism*, NATO ASI Series E: Applied Sciences, Vol. 247, Kluwer, Dordrecht, 1992.

M. Vázquez and A. Hernando, *Nanostructured and Non-crystalline Materials*, World Scientific, Singapore, 1995.
G. Timp, *Nanotechnology*, Ch. 12, AIP Press (Springer-Verlag), New York, 1998.
A. S. Edelstein and R. C. Cammarata, *Nanomaterials: Synthesis, Properties and Applications*, IoP Publishing, Bristol, 1996.
G. C. Hadjipanayis and G. A. Prinz, *Science and Technology of Nanostructured Magnetic Materials*, NATO ASI Series B: Physics, Vol. 259, Kluwer, Dordrecht, 1990.

Review articles

J. Nogués and I. K. Schuller, Exchange bias. *Journal of Magnetism and Magnetic Materials*, **192**, 203–232 (1999).
R. Skomski, Nanomagnetics. *Journal of Physics: Condensed Matter*, **15**, R841–R896 (2003).
J. I. Martín, J. Nogués, K. Liu, J. L. Vicent and I. K. Schuller, Ordered magnetic nanostructures: fabrication and properties. *Journal of Magnetism and Magnetic Materials*, **256**, 449–501 (2003).
Q. A. Pankhurst, J. Connolly, S. K. Jones and J. Dobson, Application of magnetic particles in biomedicine. *Journal of Physics D: Applied Physics*, **36**, R167–R181 (2003).
P. Tartaj, M. del Puerto Morales, S. Veintemillas-Verdaguer, T. González-Carreño and C. J. Serna, The preparation of magnetic nanoparticles for application in biomedicine. *Journal of Physics D: Applied Physics*, **36**, R182–R197 (2003).
C. C. Berry and A. C. G. Curtis, Functionalisation of magnetic nanoparticles for applications in biomedicine. *Journal of Physics D: Applied Physics*, **36**, R198–R206 (2003).